

CO $J = 3-2$ AND $J = 2-1$ OBSERVATIONS OF NGC 7027P. A. JAMINET,¹ W. C. DANCHI, AND E. C. SUTTON¹

Department of Physics and Space Sciences Laboratory, University of California, Berkeley, CA 94720

A. P. G. RUSSELL² AND GÖRAN SANDELL

Joint Astronomy Centre, 665 Komohana Street, Hilo, HI 96720

AND

J. H. BIEGING³ AND D. WILNER

Department of Astronomy, University of California, Berkeley, CA 94720

Received 1991 January 9; accepted 1991 April 29

ABSTRACT

Using the 15 m James Clerk Maxwell Telescope, we have mapped the molecular envelope surrounding the planetary nebula NGC 7027 in the $J = 3-2$ line of ^{12}CO and have observed the central position in the $J = 3-2$ line of ^{13}CO and the $J = 2-1$ lines of ^{12}CO and ^{13}CO . The $J = 3-2$ ^{12}CO map shows substantial deviations from spherical symmetry. The mass-loss rate along the nebula's polar axis appears to be about half that in the equatorial directions. Bright line wings are caused by a bipolar flow of molecular gas along the low-density axis. This gas has an outflow velocity of 23 km s^{-1} , larger than the 15 km s^{-1} expansion velocity of the bulk of the envelope. This flow is apparently driven by the pressure of the ionized region. A marked asymmetry in the $J = 3-2$ line profile toward the central position is probably due to a radiative transfer effect, which is more important in NGC 7027 than in other circumstellar envelopes due to the large velocity dispersion of neutral gas near the ionized region.

We have compared the data with CO $J = 1-0$ observations and derive new estimates for envelope parameters from a detailed model. The kinetic temperature is $30 \pm 3 \text{ K}$ at a radius of $r = 8''$ and varies with radius approximately like $r^{-0.85}$. The total mass-loss rate is $1-2 \times 10^{-4} M_{\odot} \text{ yr}^{-1}$, but the mass loss is aspherical. The CO:H₂ abundance ratio is $2^{+2}_{-1} \times 10^{-4}$, and the $^{12}\text{CO}:^{13}\text{CO}$ abundance ratio is 90 ± 25 . The radial extent of the CO emission is smaller than is consistent with the assumption of constant mass-loss rate and constant CO:H₂ ratio. This may be due to dissociation of the CO by the interstellar radiation field at characteristic radii of about $35''$ in equatorial directions and about $25''$ in polar directions. Alternatively, the mass-loss rate and/or the CO:H₂ ratio may have been smaller 8000 yr ago than they were in the more recent past.

Subject headings: interstellar: molecules — nebulae: abundance — nebulae: individual (NGC 7027) — nebulae: internal motions — nebulae: planetary

1. INTRODUCTION

Since the first detection of CO emission from planetary nebulae by Mufson, Lyon, & Marionni (1975), NGC 7027 has remained a uniquely bright source of molecular emission among planetary nebulae. A number of molecules have been detected in NGC 7027, including CO, H₂ (Treffers et al. 1976), HCN (Olofsson et al. 1982), ^{13}CO (Thronson & Mozurkewich 1983), CN (Thronson & Bally 1986), C₃H₂ (Cox, Gusten, & Henkel 1987), and HCO⁺ (Deguchi et al. 1990). Despite these observations, however, details of the physical conditions in the neutral envelope remain uncertain. This is chiefly due to the lack of observations with both high spatial resolution and high signal-to-noise ratio in multiple rotational lines from molecules. Observations in several lines are essential if such parameters as the temperature, the relative molecular abundance, and the density are to be derived unambiguously from the observations. With the advent of large submillimeter telescopes at high, dry sites and the extension of sensitive receiver technology to submillimeter wavelengths, it has recently

become possible to make moderately high spatial resolution observations of intermediate- J CO lines to complement the low- J lines observed at millimeter wavelengths.

High spatial resolution millimeter wavelength observations of NGC 7027 in the CO $J = 1-0$ line have been made by Masson et al. (1985) with the Owens Valley Radio Observatory and by Bieging, Wilner, & Thronson (1991, hereafter BWT) with the Berkeley-Illinois-Maryland Array. In our analysis we have compared our higher J data with the $J = 1-0$ data of BWT. BWT combined single-dish and interferometer data to produce images with no missing flux. The Owens Valley observations suffered from missing flux, particularly at the central velocities where the envelope appears most extended.

One previous set of observations in CO $J = 3-2$ has been reported in the literature by Phillips, White, & Richardson (1985). However, their observations suffered from lack of sensitivity, which made their line shapes unreliable, and from large beam sizes ($55''$ in $J = 3-2$ and $83''$ in $J = 2-1$). In this work we present observations in CO $J = 3-2$ with spatial resolution and sensitivity similar to those of the CO $J = 1-0$ observations of BWT, and the results of a detailed comparison of these observations.

2. OBSERVATIONS

The $J = 3-2$ observations were made primarily on 1989 August 15 at the 15 m James Clerk Maxwell Telescope, located

¹ Current address: Department of Astronomy, University of Illinois, 1002 West Green Street, Urbana, IL 61801.

² Current address: Max-Planck-Institut für Physik und Astrophysik, Institut für Extraterrestrische Physik, D-8046 Garching bei München, FRG.

³ Current address: Steward Observatory, University of Arizona, Tucson, AZ 85721.

on Mauna Kea, Hawaii, using the 345 GHz SIS receiver constructed at the University of California at Berkeley (Sutton et al. 1990). The August observations were made in a position-switching mode, using off-source positions $\pm 3'$ in azimuth from on-source positions. Pointing was checked periodically by finding the peak of the submillimeter continuum emission from NGC 7027 and other nearby compact sources. We estimate the rms pointing accuracy during our observations to have been $3''$.

A few observations were made on 1990 March 20 toward the central position for the purpose of checking the calibration of the August data. During both observing periods calibration was obtained by the chopper-wheel method in which intensities are scaled by ratioing the difference between spectra of the source and the sky to the difference between spectra of a blackbody at ambient temperature and the sky. Observations of the ambient load were made immediately following each integration in the case of the ^{13}CO observations, and following observation of seven-point and three-point strips in the case of the ^{12}CO map. However, a telescope failure in August prevented detailed checks of the calibration, especially checks of the sideband imbalance in the receiver. Significant sideband imbalance was possible in August because the receiver then used a fairly high-capacitance junction, creating a relatively high- Q resonance with the tuning backshort. In March the receiver used a low capacitance junction and was found to have a broad tuning range and, when properly tuned, negligible sideband imbalance at every frequency tested. Antenna temperatures obtained in March were found to be approximately 30% lower for the ^{12}CO $J = 3-2$ line than those obtained in August on the sources we checked, a result we attribute to sideband imbalance in August. For this work, we have rescaled the August data to reflect the March calibration. Since all of the August data used in this paper were obtained within a few hours without retuning of the receiver, the data should be internally self-consistent. We believe the March calibration to be good to $\pm 20\%$. A comparison of observations toward a number of sources showed the March calibration to be virtually identical to that found with the JCMT's 345 GHz Schottky-diode mixer. There was no statistically significant change in calibration for the ^{13}CO line between August and March.

Because NGC 7027 has a size comparable to our main beam, we present our data in units of main beam brightness temperature. A main-beam efficiency of 0.54 was derived from observations of Venus, Jupiter, and Saturn, and an extended source efficiency of 0.72 was derived from observations of the Moon. Beam maps were made on Mars, and show a circularly symmetric, Gaussian beam with a full width at half-maximum of $13''.7$ at the ^{12}CO $J = 3-2$ frequency.

The ^{12}CO and ^{13}CO $J = 2-1$ spectra were taken on 1989 October 20 with the JCMT's 230 GHz Schottky-diode mixer. These spectra were also calibrated by the chopper-wheel method, but the ratio used to fix the overall calibration was a ratio of total power integrated over the whole bandpass, rather than a ratio determined independently for each channel of the spectrometer as was the case with the $J = 3-2$ observations. The observed antenna temperatures were corrected for a main-beam efficiency of 0.65, as well as for correction factors for sideband imbalance of 0.8 in the case of ^{12}CO and 1.2 in the case of ^{13}CO . The beam at the ^{12}CO $J = 2-1$ frequency was Gaussian, with a FWHM of $21''$.

We estimate an overall calibration uncertainty of about 20%

for the ^{12}CO lines, about 30% for the ^{13}CO $J = 2-1$ line, and about 40% for the ^{13}CO $J = 3-2$ line. The larger uncertainty for the ^{13}CO calibrations reflects greater uncertainty in the sideband imbalance for both receivers and also, in the case of the $J = 3-2$ line, the larger and unbalanced atmospheric absorption at 330 GHz.

In ^{12}CO $J = 3-2$ we mapped a grid centered on the position $\alpha(1950) = 21^{\text{h}}05^{\text{m}}09^{\text{s}}.4$, $\delta(1950) = +42^{\circ}02'03''$. The grid positions were spaced at intervals of $7''$ in right ascension and declination. The map consists of 61 points formed by a 7×7 square grid with three extra points on each side of the square. Although emission is not zero at the edges of the map, it is of the same magnitude as the noise in the spectra. We observed only the central position in the ^{13}CO lines and the $J = 2-1$ ^{12}CO line.

3. RESULTS

Figure 1 presents spectra toward the central position of NGC 7027. The CO 1-0 spectrum is from BWT and, to facilitate comparison with the $J = 3-2$ data, has been convolved with a Gaussian to yield an effective resolution of $14''$ (HPBW).

Aside from a possible absorption feature at $v_{\text{lsr}} = +4 \text{ km s}^{-1}$ due to foreground gas, which some authors claim to have observed and our observations do not rule out (we discuss the question in more detail in § 4.3.5), all the features in the spectra seem to be the result of CO associated with NGC 7027. For instance, the absorption feature at $v_{\text{lsr}} = +10 \text{ km s}^{-1}$ seen in the spectra of the higher J lines is due to self-absorption by CO which is expanding directly toward us and therefore is blueshifted from the rest velocity of the nebula by its large-radius expansion velocity.

The asymmetry in the ^{12}CO $J = 3-2$ line between redshifted and blueshifted velocities, which is most apparent at velocities shifted more than 10 km s^{-1} from line center and is also present at a low level in ^{12}CO $J = 2-1$, is extraordinary; line profiles observed in other circumstellar envelopes, and profiles calculated by radiative transfer models, are generally more nearly symmetric. Nevertheless, the asymmetry can largely be accounted for by a radiative transfer effect. A detailed description of the effect is contained in § 4.3.1.

Figure 2 shows the inner spectra from our ^{12}CO $J = 3-2$ map. There are a few indications that a slight pointing offset may exist in our map. For instance, we found at the telescope that the peak in redshifted emission at $v_{\text{lsr}} = +37 \text{ km s}^{-1}$ was very sensitive to the pointing; it must arise in a region very small compared to our beam size. In Figure 2, the redshifted feature appears more prominently in spectra toward eastern positions than western ones. Probably this is due to a small pointing offset which located our map center about $2''$ west of its intended location.

The spectra toward small projected radii ($7''-10''$ from the central position) in Figure 2 show a substantial departure from spherical symmetry. To the north and west of the central position, there is little emission at velocities blueshifted by more than 5 km s^{-1} from line center, while redshifted emission is strong. Conversely, toward the southeast, redshifted emission is weak, while blueshifted emission is strong. This aspherical appearance of the envelope in the $J = 3-2$ line is consistent with the schematic picture proposed by Masson et al. (1985) for the structure of the neutral envelope. The neutral envelope is oblate in shape, with a lower density along the axis of symmetry. The ionized region is a shell that has expanded preferentially into the less dense neutral gas, thereby acquiring a

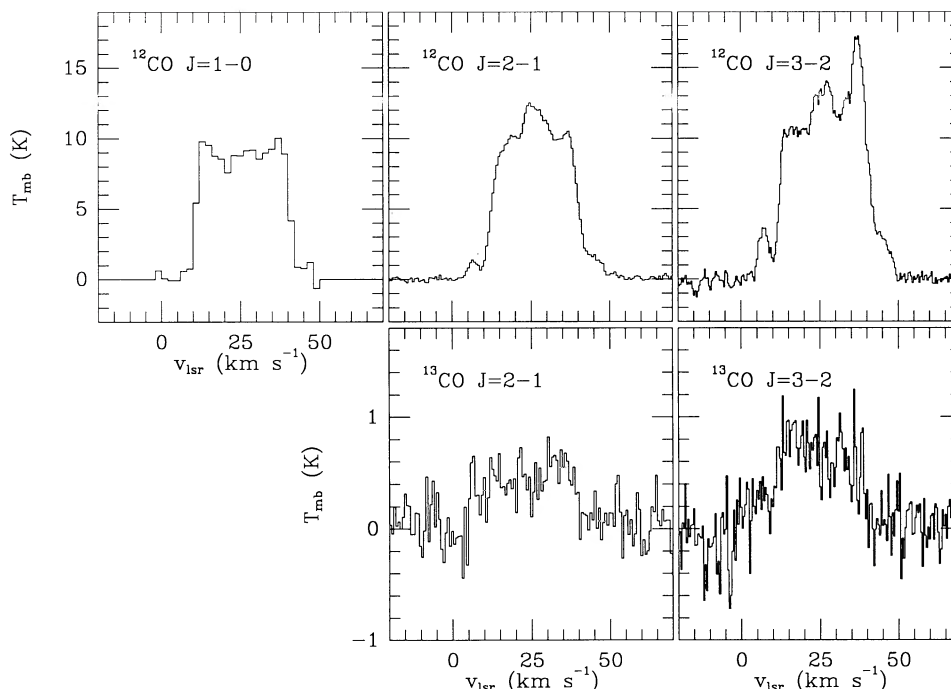


FIG. 1.—Spectra toward the central position from each of the four lines we observed, plus the $J = 1-0$ spectrum of BWT smoothed to $14''$ resolution

prolate shape; it has a total extent of about $8''$ along its minor axes and $12''$ along its major axis. The major axis is tilted by about 30° to the line of sight (Masson 1989). The $J = 3-2$ line, which is sensitive to dense gas, preferentially samples gas in the high-density plane of the neutral envelope. (Henceforth we will call the equatorial plane of the nebula, which coincides with the minor axes of the ionized region, the “high-density plane,” and the polar axis, which coincides with the major axis of the ionized region, the “low-density axis.”) The high-density plane appears blueshifted toward the SSE of the nebula center, and redshifted toward the NNW, because of the modest tilt of the low-density axis relative to our line of sight.

In Figure 3 we sketch a cross-section of NGC 7027 illustrating this geometry. The cut through the nebula illustrated in Figure 3 defines a plane which includes the NGC 7027 central star and us observers, and the low-density axis; this plane intersects the plane of the sky along the NNW-SSE axis. Other cuts would show a slightly different view of the nebula. For instance, in this cut, gas in the high-density plane emits at velocities shifted 7 km s^{-1} from line center. In other cuts, gas in the high-density plane would emit closer to line center; along the WSW-ENE axis it would emit exactly at line center. It is the existence of this high-density plane which is probably responsible for the bulge in emission in the $J = 2-1$ and $J = 3-2$ line profiles within about 7 km s^{-1} of line center. This bulge is of little significance in the $J = 1-0$ line, which is not as sensitive to density as the higher J lines.

We include in Figure 3 two boundary layers between the ionized gas and the extended molecular envelope. According to the model for photodissociation regions of Tielens & Hollenbach (1985), in any interface between H II regions and extended, dense neutral regions, there will be an intermediate region in which H_2 is self-shielded from ionization and, to a great extent, from dissociation, while CO is significantly dissociated and atomic carbon significantly ionized. Emission from H I, O I, C I, C II, CO, and vibrationally excited H_2 should all

be detectable from such a region. In the extended neutral envelope, in contrast, the gas is predominantly molecular and the molecules are in their ground vibrational states. This interface region is at most $2''$ thick in the plane of the sky; were the atomic interface region thicker, the central cavity would appear larger in maps of molecular lines.

Evidence for a layer of molecular gas which has been accelerated to larger expansion velocities by the ionized region can be found in the spectra of Figure 2. Note that $7''$ north of the central position, the blueshifted high-velocity wing ($v_{\text{lsr}} < 10 \text{ km s}^{-1}$) is considerably brighter than the redshifted wing ($v_{\text{lsr}} > 40 \text{ km s}^{-1}$), despite the prominence of redshifted emission and the depletion of blueshifted emission at velocities nearer line center. The reverse is true $7''$ south of the central position. This velocity pattern is the same as that shown by O III line emission from the ionized region, in which emission is blueshifted to the north and redshifted to the south (see Figs 6a and 6b of Atherton et al. 1979). The structure which creates this velocity pattern is illustrated in Figure 3. The high-velocity CO, which resides in or adjacent to the atomic region, and the ionized gas are both extended along the low-density axis. When we look toward the north-northwest of the central star, we see the extended molecular envelope redshifted, and the ionized, atomic, and high-velocity molecular gas blueshifted. Toward the south-southeast, the neutral envelope is blueshifted, while the ionized and high-velocity molecular gas are redshifted.

At large projected radii the spectra in Figure 2 are consistent with either an oblate or a spherically symmetric envelope. These line profiles are affected by an excitation effect. The CO $J = 3-2$ line emission is strongly biased toward hot and dense gas, and therefore toward gas closest to the central star. Along lines of sight toward large projected radii, this gas appears in the central velocity channels, tending to accentuate the emission seen in these channels.

Figure 4 presents channel maps of the $J = 3-2$ data. One

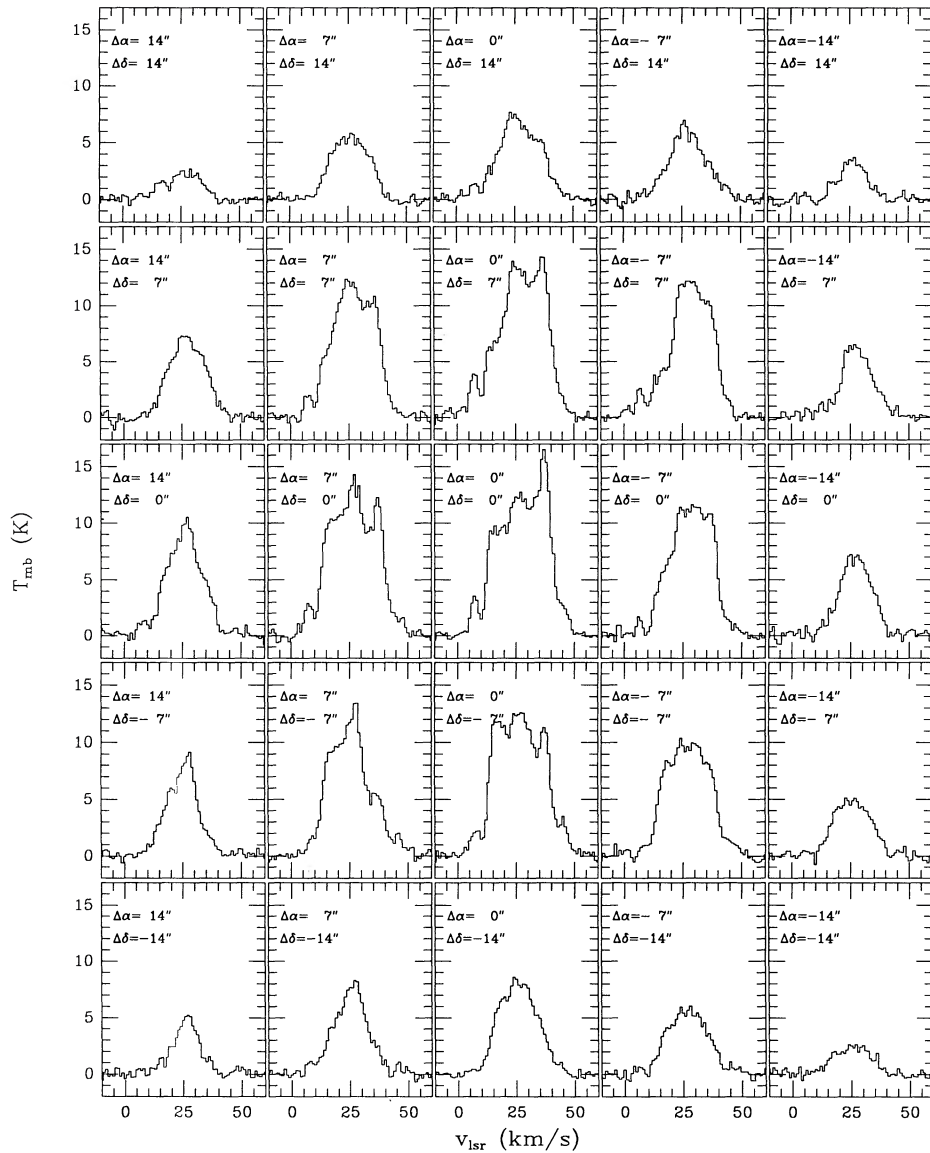


FIG. 2.—The central 25 spectra from our map of $^{12}\text{CO } J = 3-2$ emission

surprising feature of the channel maps is our failure to resolve partially the central molecular cavity at the central velocity channels; this cavity is about $9''$ in diameter, nearly as large as our beam. In the maps at the central velocities, $22 \text{ km s}^{-1} < v_{\text{lsr}} < 28 \text{ km s}^{-1}$, the emission has a single peak to the east-northeast of the central position. From our picture of the envelope geometry, two emission peaks would be expected at these velocities, one toward the ENE and one toward the WSW, because it is along the ENE-WSW line that gas in the high-density plane emits at line center. In fact, such twin peaks do occur in the $J = 1-0$ data at similar resolution, where at some velocities the WSW peak is brighter than the ENE peak. Our failure to discern separate emission peaks is probably a consequence of the small pointing offset mentioned earlier; a pointing offset that left our map center $2''-3''$ WSW of the true nebular center would account for the lack of a WSW emission peak.

4. DISCUSSION

4.1. Model Fits to the Line Profiles

To aid in the analysis of the data, we created a computer model of the NGC 7027 neutral envelope and used it to calculate fits to the observed spectra. The calculations are described in the Appendix. We started with a simple model and added complications as needed to fit the data. The simple model assumes spherical symmetry; uniform expansion velocity; a constant mass-loss rate from the central star (and therefore a molecular density proportional to r^{-2}); uniform $\text{CO}:\text{H}_2$ and $^{12}\text{CO}:\text{CO}:\text{H}_2$ abundance ratios throughout the envelope; and a power-law dependence of kinetic temperature on radius. The Sobolev (large velocity gradient) approximation is used in the calculation of the level populations.

The available data are consistent with several of these assumptions, including the assumption of a constant mass-loss

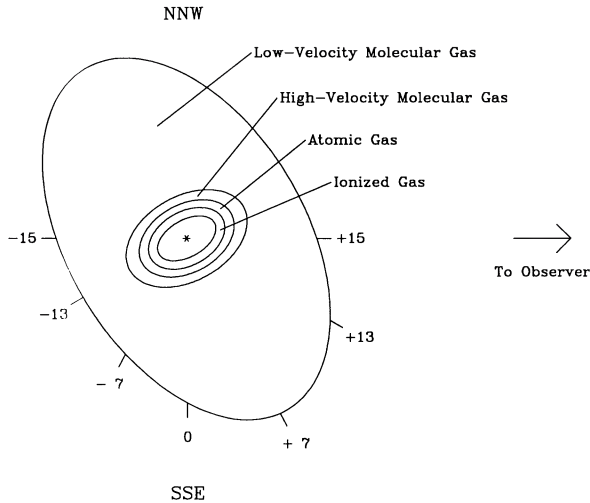


FIG. 3.—A sketch of the geometry and velocity structure of the NGC 7027 envelope, showing a cut in the plane which includes both the axis of symmetry of the envelope and Earth. This plane intersects the plane of the sky along the NNW-SSE axis of the nebula. The low-velocity molecular gas is expanding at 15 km s^{-1} , and the high-velocity molecular gas is expanding at up to 23 km s^{-1} . The numbers around the bottom half of the envelope show the velocity shift from line center of the low-velocity molecular gas for certain radial directions. Note that, while low-velocity molecular gas in the equatorial plane appears, in this cut, shifted from line center by 7 km s^{-1} , in any other planar cut which includes the observer and the central star, the equatorial plane would appear at a velocity shifted from line center by less than 7 km s^{-1} . In a cut which included the central star, the observer, and the ENE-WSW axis, the equatorial plane would appear at line center.

rate, a power-law temperature distribution, and a uniform $\text{CO}:\text{H}_2$ ratio throughout the envelope. This consistency is as much a reflection of the lack of spatial resolution in the data as of the actual uniformity of the envelope. Almost all the $J = 3-2$ line emission comes from radii between $5''$ and $15''$, yet the $J = 3-2$ beam diameter is $14''$. Without observations in multiple lines at each radius, the density, kinetic temperature, and molecular abundances cannot be determined independently, and variations in these parameters with radius are hard to detect with confidence. There is some evidence that the mass loss rate and $\text{CO}:\text{H}_2$ ratio may vary with radius; for instance, if the density in the model calculation is decreased with radius like $r^{-2.5}$ rather than r^{-2} , the observed spectra are easier to fit, in the sense that a wider range of other model parameters provide good fits to the data. Nevertheless, higher resolution observations in an excited line will be necessary before a variation in the mass-loss rate (or $\text{CO}:\text{H}_2$ ratio) with radius can be conclusively inferred.

As it happens, the assumptions of spherical symmetry and of uniform expansion velocity, as well as the assumption of negligible velocity dispersion implicit in the Sobolev approximation, do *not* seem to hold in NGC 7027. The variation in the expansion velocity, which will be discussed in § 4.3.4, appears to occur only in a narrow shell around the ionized region, and emission from this shell is unlikely to perturb much the excitation of CO elsewhere. The asphericity also likely does not much affect the validity of the calculation of the CO level populations, because the only known variation in mass-loss

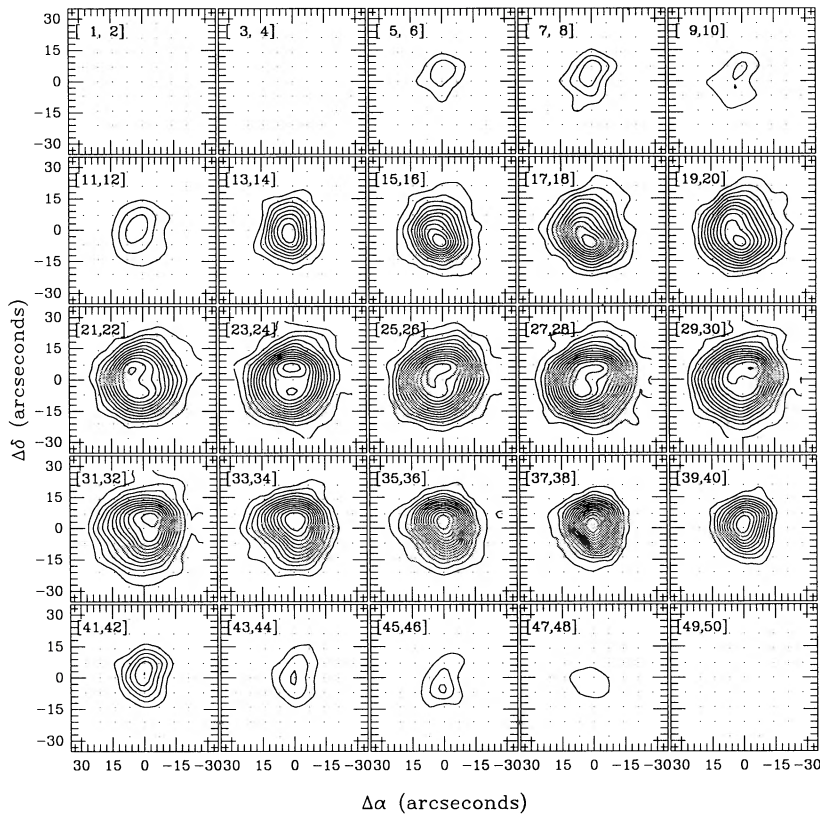


FIG. 4.—Channel maps from the $^{12}\text{CO } J = 3-2$ emission. Each map shows the integrated emission in a 2 km s^{-1} wide channel; e.g., the map labeled [5, 6] represents emission between 4.5 km s^{-1} and 6.5 km s^{-1} . Each contour represents 1 K of main-beam brightness temperature.

rate is between different radial directions, and, due to the expansion of the envelope and consequent Doppler shifts, different radial directions are not significantly radiatively coupled. The possibility of a relatively large velocity dispersion at small radii, which is discussed in § 4.3.1, raises a more serious objection to the assumptions of the model. The effect of the large velocity dispersion is to allow more CO at small radii to couple radiatively to CO at intermediate and large radii, helping to excite the CO at these larger radii. Because our model neglects this possibility, it may over-estimate the density needed at large radii to excite the CO there and consequently overestimate the mass-loss rate. Determining whether this effect is significant or not will require the performance of radiative transfer calculations which do not rely upon the Sobolev approximation.

Once the calculation of the level populations is complete, the model calculates CO line brightness, as a function of velocity, along a fine mesh of lines of sight through the nebula. The asphericity of the envelope implies that no single spherically symmetric model calculation can correctly predict the line profiles at all velocities and toward all positions. However, the spherically symmetric model calculations can still be useful guides to envelope parameters. Here again, the expansion of the envelope, because it makes regions along the line of sight that arose from different mass-loss rates emit at different velocities, eases the interpretational problem considerably; the modest tilt of the nebular axis to our line of sight also aids our analysis. For instance, emission 7 km s^{-1} from line center or closer is dominated by gas in or near the high-density plane. Emission shifted by $11\text{--}15 \text{ km s}^{-1}$ from line center, on the other hand, is dominated by gas on or near the low-density axis. Figure 3 illustrates this velocity structure. (Fig. 3 is incomplete in that it only shows one planar cut through the three-dimensional nebula. It is only in a cut through the NNW-SSE axis that the high-density plane emits at 7 km s^{-1} from line center; in a cut through the WSW-ESE axis, the high-density plane would emit exactly at line center; in other cuts, the high-density plane would emit at velocities between 0 and 7 km s^{-1} from line center.) Because of the separation in velocity of the radiation emitted from the high-density plane and the low-density axis, it is possible (to some extent) to determine parameters for these regions independently through the use of several spherically symmetric models, one of which has parameters appropriate for the high-density plane, the other of which has parameters appropriate for the low-density axis.

A typical fit of the spherically symmetric model to the observed $J = 1\text{--}0$ and $J = 3\text{--}2$ line profiles is shown in Figure 5. This model represents the best fit to the central velocity channels and therefore to the gas in the high-density plane. It is a poor fit to emission at velocities $10\text{--}15 \text{ km s}^{-1}$ from line center, because it puts too much CO along the low-density axis. The excess of CO at these velocities is most apparent in the $J = 1\text{--}0$ line because it is the least optically thick. Note that the "observed" line profiles in this figure are actually averages of the north, south, east, and west spectra at the indicated radii.

Our estimates for nebular parameters are summarized in Table 1. We have tried to make clear in the text the extent to which we trust our estimates of envelope parameters, and the reasons why. We believe that an asymmetric model calculation based on a realistic source geometry, such as that sketched in Figure 3, would largely confirm the conclusions of this paper, given the available data.

TABLE 1
PARAMETERS OF THE NGC 7027 NEUTRAL ENVELOPE

Parameter	Value
v_{lsr}	25.2 km s^{-1}
v_{exp} , extended envelope	15.2 km s^{-1}
v_{exp} , small radii ^a	23 km s^{-1}
Δv , extended envelope ^b	$< 0.8 \text{ km s}^{-1}$
Δv , small radii ^b	2.0 km s^{-1}
Width of high-velocity CO shell ^c	$0\%6$
T_{kin} at $r = 8''$	$30 \pm 3 \text{ K}$
Radial dependence of T_{kin}	$r^{-0.85 \pm 0.10}$
Mass-loss rate, high-density plane	$2.2 \pm 0.7 \times 10^{-4} M_{\odot} \text{ yr}^{-1}$
Radial extent of CO in dense disk	$> 30''$
Mass-loss rate, to fit low-density axis	$1.0^{+1.0}_{-0.5} \times 10^{-4} M_{\odot} \text{ yr}^{-1}$
Radial extent of CO along low-density axis	About $25''$
CO:H ₂ abundance ratio	$2^{+2}_{-1} \times 10^{-4}$
¹² CO: ¹³ CO abundance ratio	90 ± 25
Mass of observable envelope ^d	$1.4^{+0.8}_{-0.4} M_{\odot}$

^a Along the line of sight. The expansion velocity is probably smaller in directions orthogonal to the line of sight. See § 4.3.4.

^b Δv is a measure of the turbulent velocity dispersion; it is defined as in Morris, Lucas, & Omont 1985.

^c Based on the column density of high-velocity CO necessary to produce observed line wings. See § 4.3.4.

^d Observable envelope extends to $r = 4 \times 10^{17} \text{ cm}$.

4.2. Parameters Determined from Line Intensities

4.2.1. Kinetic Temperature and CO Abundance at Small Radii

As is generally the case when the brightness temperatures of different lines are approximately the same, the ¹²CO lines could be fitted only by moderately optically thick emission. Furthermore, all of our observed lines appear to be thermalized out to $r = 10''$ or larger. For optically thick and thermalized lines, the observed brightness temperature is strongly dependent on the kinetic temperature and only weakly dependent on other envelope parameters. For this reason, our model fits are sensitive to the kinetic temperature at small radii. We estimate the kinetic temperature to be $30 \pm 3 \text{ K}$ at the radius $r = 8''$.

The CO column density is sufficiently large to make the lines moderately optically thick but cannot be too large, or the $J = 1\text{--}0$ line would have the same intensity and line shape as the higher J lines. The $J = 1\text{--}0$ line, which is the least optically thick, is mildly sensitive to the CO column density at small radii, while the optically thick $J = 3\text{--}2$ line profile is almost independent of the column density at small radii. The ratio of line intensities fixes the column density of CO in the low- J levels within about 40%.

Corroboration of this estimate of the CO column density is provided by an examination of the line profiles, with special attention to the lack of asymmetry in the $J = 1\text{--}0$ line, and the modest asymmetry of the $J = 2\text{--}1$ line, compared to the substantial asymmetry in the $J = 3\text{--}2$ line. The lack of a significant asymmetry in the observed $J = 1\text{--}0$ line profile requires a radial optical depth (of gas lying along our line of sight to the central star) that is at most unity. On the other hand, the tangential optical depth (of gas in the plane of the sky and the central star) may not be significantly less than one, or the $J = 1\text{--}0$ line in a $14''$ beam would have a double-peaked line profile, largely because of the presence of the central cavity

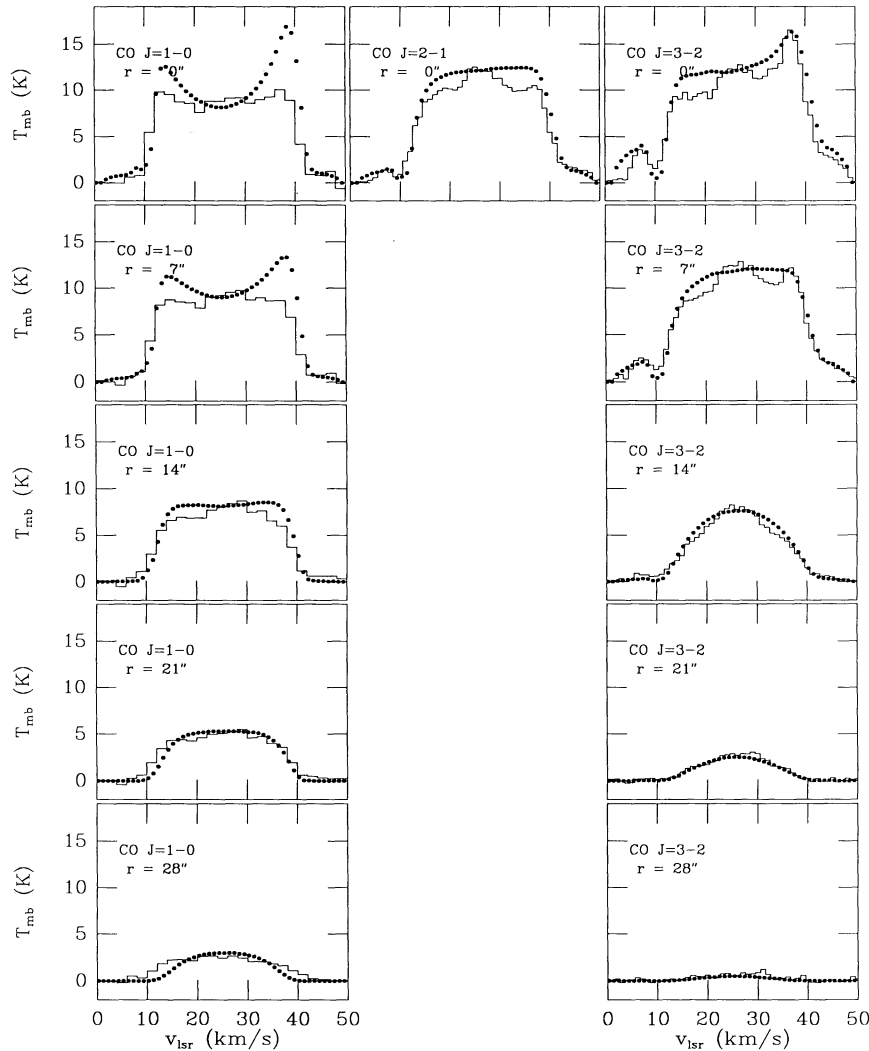


FIG. 5.—Radial dependence of $J = 1-0$ (left column) and $J = 3-2$ (right column) line profiles, the $J = 2-1$ spectrum (central column), and a sample spherically symmetric model fits to the data (dots). The model shown here had $T_{\text{kin}} = 31$ K at $r = 8''$ with an $r^{-0.85}$ radial dependence, a mass-loss rate of $2.2 \times 10^{-4} M_{\odot} \text{ yr}^{-1}$, and a $\text{CO}:\text{H}_2$ ratio of 2.2×10^{-4} , and a photodissociation radius of $35''$. These parameters are the best fit to the gas in the high-density plane, which appears in the central velocity channels. The “observed” line profiles shown here are averages of profiles from the north, south, east, and west of the central position at the radii shown. The $J = 1-0$ data is from BWT; their data have been smoothed to the same spatial resolution as the $J = 3-2$ data.

which affects the central velocity channels most strongly. Instead, the line profile appears flat-topped, implying a tangential optical depth at least of the order of unity. Since the radial opacity is much greater than the tangential opacity in a spherically symmetric, uniformly expanding envelope, the envelope must be aspherical, with a smaller rate of mass loss along our line of sight than in the plane of the sky. These measures of line opacity strongly constrain the CO column density. Reexpressed in terms of a mass-loss rate, the CO column density corresponds to a mass loss rate of $6.0 \pm 1.5 \times 10^{-7} M_{\odot} \text{ yr}^{-1}$, just in CO molecules. We express the column density in terms of a mass-loss rate, rather than as a number per unit area, so the result will be independent of parameters like the radius at which photodissociation of CO occurs.

4.2.2. Kinetic Temperature and Density toward Large Projected Radii

At radii of about $20''$ the envelope is no longer dense enough to excite CO to the higher J levels, and only the $J = 0$ and $J = 1$ levels are not subthermally populated. Because so much

CO is in these levels, the $J = 1-0$ line becomes more optically thick, and the intensity of this line becomes a good measure of the kinetic temperature. The kinetic temperature falls with radius more slowly than $r^{-0.95}$ but faster than $r^{-0.75}$. This variation is similar to that predicted by Deguchi et al. (1990) for NGC 7027, and slightly more rapid than that in IRC +10216 (Kwan & Linke 1982).

The radius at which the population of the $J = 3$ and $J = 2$ levels becomes subthermal is strongly sensitive to the density. However, in our $14''$ beam it is difficult to determine exactly how the $J = 3-2$ emission declines with radius. For this reason the total mass-loss rate is less well-determined than other important model parameters. A mass-loss rate of $2 \times 10^{-4} M_{\odot} \text{ yr}^{-1}$ in the high-density plane, which emits in the central velocity channels, can fit the observed radial dependence of both the $J = 3-2$ and $J = 1-0$ lines quite well, as is illustrated in Figure 5. A mass-loss rate of $1 \times 10^{-4} M_{\odot} \text{ yr}^{-1}$ is too small to fit the extent of the $J = 3-2$ emission, unless radiative transfer of CO line photons from small radii to large radii contrib-

utes significantly to the excitation. This possibility is neglected by our model, which neglects radiative transfer between radii when calculating level populations. The mass-loss rate is less than $3 \times 10^{-4} M_{\odot} \text{ yr}^{-1}$.

The mass-loss rates quoted here are appropriate for the high-density plane, which emits in the central velocity channels, because it is in these channels that the nebula is extended and in which the radial dependence of the emission can be studied. We cannot directly calculate the mass-loss rate along the low-density axis from the available data; to determine this parameter quantitatively will probably require observations with higher spatial resolution and/or a model that explicitly accounts for the asphericity of the envelope. We can estimate the mass-loss rate along our line of sight to NGC 7027 based on the amount of CO needed to produce the observed level of emission: a modest opacity is needed in the $J = 1-0$ line to minimize the $J = 1-0$ line asymmetry, but a larger opacity in the $J = 3-2$ line is necessary to emphasize the $J = 3-2$ line asymmetry. However, each of these estimates is fraught with uncertainty. The line opacities, for instance, depend on the radial dependence of the velocity dispersion and expansion velocity, neither of which is well determined. Our best estimate is that the mass-loss rate is about a factor of 2 lower along the low-density axis than in the high-density plane. The data are somewhat confusing, however; the lack of $J = 1-0$ line asymmetry and the shallowness or absence in all three lines of self-absorption at $v_{\text{lsr}} = 10 \text{ km s}^{-1}$ suggests that little cold gas exists at large radii along our line of sight, but the large $J = 3-2$ line asymmetry suggests that a great deal of warm CO exists at small radii along our line of sight. One possible explanation for this apparent paradox, that CO might be dissociated to a smaller radius along our line of sight than in the plane of the sky, is discussed in § 4.2.4.

4.2.3. CO:H₂ Abundance Ratio

Using the estimate for the CO abundance derived from observations toward small radii and the estimate for the mass-loss rate derived from observations toward large radii, we can estimate a CO:H₂ ratio under the assumption that the mass-loss rate and the CO:H₂ ratio were constant. A mass-loss rate of $2 \times 10^{-4} M_{\odot} \text{ yr}^{-1}$ corresponds then to a CO:H₂ ratio of 2×10^{-4} . This CO:H₂ ratio is rather less than would be expected from C:H and O:H ratios observed in the ionized region, a point which is discussed in § 4.4.

4.2.4. The Radial Extent of the CO Distribution

Toward very large radii, $r \geq 30''$, the $J = 1-0$ emission cuts off sharply. Either the $J = 1$ level becomes subthermally populated at this radius, or there is a sharp drop in the CO abundance at this radius. Our model indicates that the $J = 1$ level would not become sufficiently subthermal at this radius if model parameters appropriate at small radii also hold at these larger radii. For instance, the mass-loss rate would have to fall to less than $1 \times 10^{-4} M_{\odot} \text{ yr}^{-1}$, about half the mass-loss rate at smaller radii, to make the density small enough at $r = 30''$ to account for the observed lack of emission. Gas at this radius, by the way, would have been lost by the central star about 8000 yr ago.

An alternative possibility is that photodissociation of the CO by interstellar radiation occurs near this radius. This explanation, in addition to helping explain the observed radial extent of the emission, helps our model to fit the observations toward small projected radii, in which the lack of $J = 1-0$ line

asymmetry and shallowness of the $J = 3-2$ self-absorption feature suggest that opacities of cold gas at large radii are small along our line of sight to NGC 7027, while the large asymmetry in the $J = 3-2$ line profile suggests that CO is much more abundant at small radii. CO at small radii contributes little to the $J = 1-0$ line opacity, because the high densities and temperatures obtained at these radii mean that only a small fraction of the CO lies in the $J = 0$ and $J = 1$ levels; it is possible to have much larger opacities in the $J = 3-2$ line than $J = 1-0$ line at small radii, because of the much larger A -coefficient of the higher J line, as well as the larger statistical weight of the levels. At radii larger than about $20''$, however, the $J = 1-0$ line opacity is larger than the $J = 3-2$ line opacity, because the high- J levels are all subthermally populated. The existence of a self-absorption feature at $v_{\text{lsr}} = 10 \text{ km s}^{-1}$ in the $J = 2-1$ and $J = 3-2$ lines but not in the $J = 1-0$ line, tells us that CO along our line of sight to NGC 7027 definitely extends out to radii at which the $J = 2$ level is subthermally populated but suggests that it does not extend to radii at which the $J = 1$ level becomes subthermally populated. This radius is likely to be the equivalent, in the plane of the sky, of an angular radius of about $25''$. Photodissociation of CO at about $35''$ in the direction of the high-density plane, and at a radius along the low-density axis which would correspond to about $25''$ in the plane of the sky, seems to be the easiest way to account for the observed emission.

Calculations of the radius at which CO could be expected to be dissociated in NGC 7027 predict slightly larger characteristic radii than $35''$, though the difference is probably within the uncertainty of the calculation. For a mass-loss rate of $2 \times 10^{-4} M_{\odot} \text{ yr}^{-1}$ and a CO:H₂ ratio of 2×10^{-4} , Mamon, Glassgold, & Huggins (1988) predict a photodissociation radius of $6.67 \times 10^{17} \text{ cm}$, which at the distance of NGC 7027 corresponds to a radius of $51''$. (The mass-loss rates listed by Mamon et al in their Table 3 must be corrected for the smaller CO:H₂ ratio obtained in NGC 7027 than in their model envelope, because the CO is predominantly self-shielded, and the smaller CO:H₂ ratio leads to less effective self-shielding.) Given the uncertainty in the distance to NGC 7027, in the intensity and spectral hardness of interstellar radiation near NGC 7027, and in the dependence of the mass-loss rate with radius, the difference between $50''$ and $35''$ may not be significant. An additional source of uncertainty is the possibility that the CO:H₂ abundance ratio may vary with radius in NGC 7027, as we suggest in § 4.4; if the CO:H₂ ratio were smaller at large radii, then the dissociation radius predicted by Mamon et al. would be in better agreement with our model fit. Moreover, the dependence of dissociation radius upon mass-loss rate was calculated by Mamon et al. only for a spherical geometry; for an aspherical envelope like NGC 7027, the dissociation radius would probably be smaller in the high-density plane than predicted by Mamon et al., due to the reduced shielding against photons arriving tangentially toward the high-density plane. The difference in suggested photodissociation radii between the high-density plane and low-density axis is probably consistent with the difference in their mass loss rates.

4.3. Details of the Line Profiles

4.3.1. The Asymmetry in the $J = 3-2$ Line

The red/blue asymmetry in the $J = 3-2$ line toward the nebula center is more extreme than the asymmetries previous radiative transfer calculations have predicted, and indeed it is

difficult to generate such a large asymmetry in a spherically symmetric envelope. However, an asymmetry substantially larger than those previously predicted is possible, even in the spherically symmetric case, for an appropriate set of envelope parameters. Extreme asymmetry requires (1) that the line of interest has a large opacity, so as to make as great as possible the difference in radius between the blue- and redshifted emitting regions at a given velocity shift from line center; (2) that the line arise from a state in which the excitation is strongly sensitive to radius, as is the case for collisionally excited gas in which the density is about equal to or less than the critical density of the line; and (3) that the velocity dispersion in the gas be significant compared to the gas expansion velocity. All of these conditions hold in NGC 7027 in the case of the $J = 3-2$ line. The asymmetry occurs preferentially in the $J = 3-2$ and, presumably, the $J = 4-3$ line, because, first, these lines attain greater opacities than lower J lines due to their much larger A -coefficients (the A -coefficient of the $J = 3-2$ line is a factor of 34 larger than that of the $J = 1-0$ line) and the greater statistical weights of their levels, and, second, because their line excitation temperatures depend more strongly on radius than do those of the lower J lines, due to the greater sensitivity of the high- J lines to the density.

Figure 6 illustrates the velocity dependence of the line profile asymmetry for an optically thick line in a source with a geometry like that of NGC 7027. In case (a), in which emission occurs at a velocity shifted from line center by the gas expansion velocity, the blueshifted emission is completely obscured by gas at the largest radii, which in a high- J line is likely to be in equilibrium with the cosmic microwave background and therefore invisible. At the corresponding redshifted velocity, however, most of the emission region lies at small radii, where the gas is hot and bright. In case (b), in which the observed velocity is shifted from line center by slightly less than the gas expansion velocity, the observed redshifted emission is larger than in case (a) if the source is unresolved, because the fraction of the beam subtended by the emitting region is increased while the surface brightness is not significantly reduced. The blueshifted emission is also brighter, but for the most part still arises from cold, dim gas. In NGC 7027 we do see significant blueshifted emission at this velocity in the $J = 3-2$ line, mainly because the velocity dispersion is not independent of radius,

but instead is large (perhaps $2-3 \text{ km s}^{-1}$) at small radii and much smaller (less than 1 km s^{-1}) at large radii; this allows some emission from small radii to peek through, especially (we predict) along lines of sight directly toward the central star. Emission from small radii can escape more easily in the less optically thick $J = 1-0$ line than in the $J = 3-2$ line; this is, in part, why the $J = 3-2$ self-absorption feature appears in channels at $v_{\text{lsr}} = 9, 10,$ and 11 km s^{-1} , while significant emission occurs in the $J = 1-0$ channel at $v_{\text{lsr}} = 11 \text{ km s}^{-1}$ (see Fig. 5). Finally, case (c) illustrates the asymmetry at velocities nearer line center. An asymmetry remains because along any line of sight the blueshifted emitting region is at a larger radius than the redshifted emitting region. However, the asymmetry is small and disappears as the velocity tends toward line center. Note that, if the velocity dispersion were zero, there could be no asymmetry at any velocity shift from line center except precisely the gas expansion velocity.

As can be inferred from Figure 6, the magnitude and velocity dependence of the line profile asymmetry are strongly affected by magnitude of the velocity dispersion. The magnitude of the $J = 3-2$ line asymmetry in NGC 7027 is evidence for a velocity dispersion of as much as 3 km s^{-1} at small radii. A velocity dispersion of this size also reproduces the velocity at which the redshifted emission peaks, about 12 km s^{-1} from line center. One interesting result of the model is that, in order to reproduce the magnitude of the asymmetry, the velocity dispersion must be significantly greater than 1 km s^{-1} out to radii at least several arcseconds larger than the outer radius of the high-velocity molecular gas. It seems unlikely that any event coincident with or following the formation of the ionized region could have created turbulence at radii so much larger than the radius of the shock front separating the high-velocity gas from the low-velocity gas. We can speculate that this extended turbulence in the low-velocity gas may be a relic of a high-velocity molecular wind which, during the proto-planetary nebula phase, disturbed the low-velocity gas.

Despite indications from our modeling that the extreme asymmetry in the $J = 3-2$ line can largely be accounted for by radiative transfer effects, it is possible that a difference in excitation or abundance between the red- and blueshifted sides of the envelope contributes to the line asymmetry. Such an envelope asymmetry would be different from the asymmetry

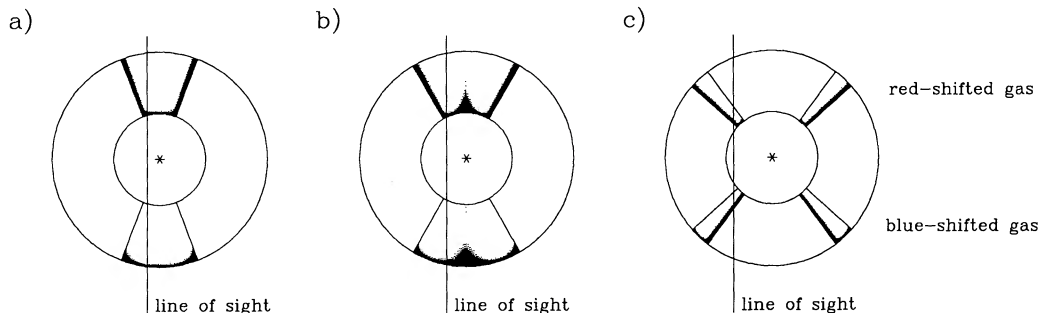


FIG. 6.—Illustration of the velocity dependence of the red-blue line profile asymmetry in a spherically symmetric envelope with a central cavity and a significant velocity dispersion, observed in an optically thick line. The radial lines define regions in which gas molecules expanding radially at 15 km s^{-1} have projected velocities within 1 km s^{-1} of some observed velocity. The heavy black shaded region in which the optical depth between the emitting point and the observer is less than unity. The particular lines of sight shown are arbitrary; almost any line of sight will produce an asymmetry, and so an asymmetry will exist even if the observing beam does not resolve the envelope. (a) Observed velocity is 15 km s^{-1} from line center. The blueshifted emission region is at a much larger radius than the redshifted emitting region. (b) Observed velocity is 14 km s^{-1} from line center. For an unresolved source, the redshifted emission is generally brighter than in case (a), because the emitting region subtends a larger fraction of the beam, and the surface brightness is only slightly reduced. (c) Observed velocity is 11 km s^{-1} from line center. There is still an asymmetry, because along every line of sight the blueshifted emitting region is at a larger radius than the redshifted emitting region. However, the asymmetry is small, and tends toward zero as the velocity approaches line center.

sketched in Figure 3; the geometry sketched in Figure 3 is aspherical but retains inversion symmetry about the central star. The question of whether radiative transfer effects, or excitation or abundance asymmetries, cause the $J = 3-2$ line asymmetry could be answered by a high signal-to-noise ratio observation of the ^{13}CO $J = 3-2$ line. If radiative transfer effects are responsible, then the optically thin ^{13}CO line should appear symmetric. If density or temperature or abundance variations cause the line asymmetry, then the ^{13}CO line should share the asymmetry. Unfortunately our ^{13}CO observations lack the signal-to-noise ratio needed to resolve the question.

4.3.2. *The Lack of $J = 1-0$ Line Asymmetry*

Our model tends to generate an asymmetry in the $J = 1-0$ line profile, as well as one in $J = 3-2$. These asymmetries have somewhat different origins. About 1.5 K of the $J = 1-0$ line asymmetry is due to the effect of continuum emission from the ionized region. This continuum emission is of only minor significance for the larger $J = 3-2$ line asymmetry, to which it contributes only about 0.2 K. The continuum emission causes an asymmetry in the $J = 1-0$ line because the blueshifted CO is optically thick to the continuum and absorbs it, while the ionized region is optically thin to the redshifted CO and does not significantly absorb it. Thus at velocities redshifted from line center by the expansion velocity, we see emission from both the CO and the ionized region; at the corresponding blueshifted velocity, we see only the CO. Were there no continuum emission from NGC 7027, the line asymmetry we predict in the $J = 1-0$ line would be small for the model parameters which best fit NGC 7027.

The $J = 1-0$ line does not show a significant asymmetry in the spectra with $14''$ resolution. An asymmetry does appear in the $J = 1-0$ map with the full resolution, where the line profile toward the central position is double-peaked and the red peak has about 15% more flux than the blue peak. However, the observed asymmetry is much smaller than that predicted by spherically symmetric models which can fit the emission at the central velocity channels.

The failure of the $J = 1-0$ line to show a larger asymmetry is evidence that opacities in the $J = 1-0$ line along our line of sight to the ionized region are modest at all velocities. We estimate that the total optical depth in the $J = 1-0$ line between us and the ionized region is on the order of 1-5. This is surprisingly small, given that tangential optical depths in the $J = 1-0$ line for gas in the plane of the sky must be on the order of 1 in order to reproduce the magnitude of the $J = 1-0$ emission in the central velocity channels. For comparison, the spherically symmetric model fit shown in Figure 5 tangential optical depths in the $J = 1-0$ line of 0.7-1.1, depending on radius, and a radial optical depth in this line of about 10. The $J = 3-2$ line has tangential optical depths between 1 and 4 and radial optical depth of about 20. Accounting for the apparently modest line opacity in the $J = 1-0$ line requires a factor of 2-10 less CO along our line of sight to NGC 7027 than must exist along directions orthogonal to our line of sight (in order to account for the observed intensity, and line intensity ratios, in off-center observations).

The uncertainty in our estimates of the CO opacity and the asymmetry in CO radial columns is large, because of uncertainty regarding the velocity structure and radial extent of the neutral envelope. If the velocity dispersion is small and if CO is dissociated to a small radius, then continuum emission from the ionized region may be largely unobscured by nebular CO,

even if the opacity in the CO line is high where it does obscure the ionized region. On the other hand, if the velocity dispersion is large and CO is not dissociated to a small radius, then the ionized region will be obscured, and the opacity in the CO line must be small to account for the lack of line asymmetry. This would require a rather extreme envelope asymmetry.

A large asymmetry in the CO radial columns does not necessarily imply an equally large asymmetry in mass-loss rates, if the extent of the CO distribution is determined by photodissociation due to interstellar UV. In this case, CO along the low-density axis will be dissociated to a smaller outer radius by interstellar radiation, and to a larger inner radius by radiation from the central star and planetary nebula, than CO in the high-density plane. Under these circumstances, an asymmetry in mass loss rate of only a factor of 2 or 3 could produce an asymmetry of as much as a factor of 5 in the CO radial columns.

4.3.3. *The $J = 3-2$ Self-Absorption Feature*

The depth and shape of the absorption feature at $v_{\text{lsr}} = 10$ km s $^{-1}$ in the $J = 3-2$ and $J = 2-1$ lines cannot easily be reproduced by the spherically symmetric model. The model tends to generate absorption features that dip below the apparent continuum. This is because even for the largest mass-loss rates the excitation temperature between the $J = 2$ and $J = 3$ levels approaches the temperature of the cosmic microwave background at radii of about $20''$. In order to fit the observed radial extent of the CO in the plane of the sky, the spherically symmetric model requires the existence of CO at radii up to nearly $30''$, and there is then enough CO between $20''$ and $30''$ to make the radial opacity in the $J = 3-2$ line larger than unity.

A shallower absorption feature, like the one we actually observe, can be reproduced in several ways. If the expansion velocity and the velocity dispersion are sufficiently larger at small radii than at large radii, then there can be emission at $v_{\text{lsr}} = 10$ km s $^{-1}$ along lines of sight for which there is no absorption. An expansion velocity of 23 km s $^{-1}$ at small radii such as is necessary to reproduce the high-velocity wings, combined with a velocity dispersion that reaches 3-4 km s $^{-1}$ at small radii and falls to less than 1 km s $^{-1}$ at intermediate radii, can together account for the depth and shape of the absorption feature, as long as CO does not exist at radii larger than $30''$. If the CO extended to infinite radius, then cold CO would obscure the whole nebula.

A second possible explanation for the shallowness of the absorption feature is that the CO along the line of sight has a smaller radial extent than the CO orthogonal to the line of sight. This is consistent with the picture of the envelope geometry discussed in § 3, if the radial extent of the CO is determined by dissociation by the interstellar radiation field; then the less dense gas along the axis of the nebula would be dissociated at smaller radii than the denser gas in the equatorial plane. If gas in the equatorial plane is dissociated at a radius of about $35''$, as discussed in § 4.2.4, it would clearly be dissociated at still smaller radii along the low-density axis, which is only slightly tilted to the line of sight.

Probably both possibilities contribute to the depth of the absorption feature. There are reasons other than the absorption feature to believe that both possibilities are realized in NGC 7027. In particular, a large increase in the expansion velocity at small radii is necessary to account for the emission in the high-velocity wings.

4.3.4. The High-Velocity Line Wings

It is possible to produce high-velocity line wings even in circumstellar envelopes with a uniform expansion velocity if the velocity dispersion is significant, because the velocity dispersion causes some gas to appear in emission at velocities more extreme than the expansion velocity (e.g., Schonberg 1988, Fig. 10). However, this mechanism cannot readily produce wings as bright as the observed NGC 7027 line wings, nor can it easily reproduce the observed shape of the line wings. In light of the source geometry discussed in § 3, the brightness of the wings, and the bipolarity of the wings which matches the bipolarity of the ionized region, it is clear that the wings are sampling CO which has acquired large expansion velocities from association with the ionized region. Because redshifted emission, which is not contaminated by foreground absorption as the blueshifted wing may be, appears at velocities as large as 24 km s^{-1} from line center, it is necessary to assume expansion velocities of about 23 km s^{-1} to account for the wings.

Such an expansion velocity is probably consistent with the expansion velocity of the ionized gas. Masson (1989) estimates that the ionized region is expanding at a velocity of about 17.6 km s^{-1} along its minor axis, but perhaps as much as 50% faster along the major axis. An expansion velocity as fast as 23 km s^{-1} for the ionized gas along the low-density axis is probably consistent with the O III line profiles of Atherton et al. (1979) and the millimeter-wavelength hydrogen and helium recombination line profiles of Vallee et al. (1990). Interestingly, this velocity would be similar to the expansion velocities of other planetary nebulae; Zuckerman & Aller (1986) point out that planetary nebulae typically have expansion velocities of about 24 km s^{-1} , compared to typical expansion velocities of 16 km s^{-1} for the precursor AGB star envelopes.

The great pressure in the ionized region, where electron temperatures of 14,000 K (Basart & Daub 1987) and densities of $7 \times 10^4 \text{ cm}^{-3}$ (Masson 1989) are obtained, exerts sufficient force to accelerate the neutral gas to a velocity of 23 km s^{-1} . By equating the force exerted by the ionized region on the neutral gas with the rate of momentum transfer to the neutral gas, and using the mass-loss rate derived from our model fits to the line profiles, we can estimate the velocity to which the neutral gas would be accelerated. The force exerted by the ionized region is $F = 4\pi r_{\text{out}}^2 nkT$, where r_{out} is the outer radius of the ionized region, n is the number density, and T is the temperature in the ionized region. The momentum per unit time imparted to the accelerated neutral gas is $4\pi r_{\text{shock}}^2 \rho u v_{\text{shock}}$, where r_{shock} is the radius of the shock front bounding the accelerated gas from the low-velocity gas, ρ is the mass density of the low-velocity gas at the shock front, u is the difference in expansion velocities between the accelerated gas and the extended neutral gas, and v_{shock} is the difference in expansion velocity between the shock front and the low-velocity gas. The momentum term is actually independent of r_{shock} and depends only on the assumed mass-loss rate, u , and v_{shock} , since ρ falls like the radius squared. Approximating $v_{\text{shock}} \approx 4u/3$, which is the result for a nonradiative shock in an ideal gas in which rotational degrees of freedom are not excited (Spitzer 1978), using a mass-loss rate of $2 \times 10^{-4} M_{\odot} \text{ yr}^{-1}$, taking $r_{\text{out}} \approx 6.5 \times 10^{16} \text{ cm} = 5''$ along our line of sight to the central star, and using the values for n and T given above, we find a value for u of 7.7 km s^{-1} , which corresponds to an expansion velocity for the high-velocity CO of about 23 km s^{-1} . For the gas orthogonal to the line of sight, where the outer radius of the ionized

region is slightly smaller and the mass-loss rate slightly larger, similar analysis gives $u \approx 5 \text{ km s}^{-1}$, or a high-velocity molecular gas expansion velocity of about 20 km s^{-1} .

Our fits to the brightness of the high-velocity CO emission allow us to estimate the column density of CO which has been accelerated to this velocity. We cannot estimate other parameters of the high-velocity gas, even though we have observations of the wings in three CO lines, because none of the three low- J lines is sensitive to the density, and their functional dependence on the kinetic temperature is too similar to that on the column density to reasonably constrain both parameters. A column of CO which provides an excellent model fit to the line wing emission can always be found, as long as the kinetic temperature of the gas is greater than the 33 K excitation energy of the $J = 3$ level and the density significantly greater than the 10^4 cm^{-3} needed to excite the $J = 3$ level. To estimate the column density, we have extrapolated the density, CO:H₂ ratio, and kinetic temperature derived by our spherically symmetric model for the low-velocity envelope to the radius of the high-velocity gas. In this case, under the assumption of a sudden transition from atomic to molecular gas at a radius $r = 5''$, the shell of molecular gas which is expanding at a velocity of 23 km s^{-1} must be 0.6 thick in order to present the appropriate column of CO. This is the origin of the entry in Table 1 labeled "Width of high-velocity CO shell."

This estimate of the thickness of the high-velocity molecular shell should not be taken too literally; it is intended as an approximate description of the amount of molecular gas which has been accelerated, not as an accurate measure of the width of the high-velocity shell. In reality an appreciable fraction of the accelerated gas will be atomic, and the density, CO:H₂ ratio, and kinetic temperature obtained in this shell will differ from the values assumed by our calculation. Both of these sources of uncertainty make difficult an accurate estimate of the actual thickness of the shell of accelerated gas. However, our estimate must be approximately correct. If we suppose that half the accelerated gas is atomic, so that the shell of accelerated gas is 1.2 thick, and that $v_{\text{shock}} = 10 \text{ km s}^{-1}$, then we find that acceleration of the gas must have begun about 500 yr ago. This is consistent with the upper limit of 700–1000 yr for the age of the ionized region derived by dividing the radius of the ionized region by the expansion velocity of the gas.

An alternative explanation for the high-velocity molecular gas is that it may be the relic of a high-velocity wind ejected during the proto-planetary nebula phase and not yet completely ionized or decelerated by contact with the low-velocity envelope. This explanation cannot be ruled out. However, we think it implausible. It is clear that the pressure in the ionized region is vastly greater than the pressure in the neutral envelope, and therefore the ionized gas must be accelerating the neutral gas. If the high-velocity molecular gas achieved its high expansion velocity before the formation of the ionized region, and therefore has not been accelerated by the ionized gas, then the ionized region must be expanding 4–8 km s^{-1} faster than 23 km s^{-1} , because only the inertial force of lower pressure ionized gas. Such high expansion velocities for the ionized gas are inconsistent with the observed line-widths in the ionized region; these line widths are typically about 45 km s^{-1} , and the expansion velocity is unlikely to be more than half the observed line width (Atherton et al. 1979; Vallee et al. 1990). Further, there is no clear physical reason why the remnants of a post-AGB high-velocity wind should be expanding at 23 km

s^{-1} , approximately the right velocity for gas in the extended envelope to have been accelerated in the ionized gas; the post-AGB winds in other sources are considerably faster, at about 50 km s^{-1} in CRL 2688 (Kawabe et al. 1987) and 190 km s^{-1} in CRL 618 (Gammie et al. 1989).

4.3.5. A Possible $+4 \text{ km s}^{-1}$ Absorption Feature

It has been suggested by Deguchi et al. (1990) and others that CO line profiles from NGC 7027 are mildly contaminated by emission from an extended foreground cloud at $v_{\text{lsr}} = +5 \text{ km s}^{-1}$. Pottasch et al. (1982) saw absorption at this velocity in H I toward NGC 7027 and four radio continuum sources up to $25'$ away. This absorption could not have been generated by matter lost by NGC 7027 itself. While there may well be extended emission at this velocity in CO $J = 1-0$, we found no evidence for extended emission in the $J = 3-2$ line. However, as inspection of the model fits to the high-velocity line wings shown in Figure 5 shows, there is some evidence for an absorption feature near this velocity. The model fits suggest that emission from the blueshifted wing should extend to about $v_{\text{lsr}} = +1 \text{ km s}^{-1}$, whereas the observed emission cuts off abruptly at $v_{\text{lsr}} = +5 \text{ km s}^{-1}$. This discrepancy is most likely due to absorption by foreground gas. If foreground gas does not absorb emission at $v_{\text{lsr}} < +5 \text{ km s}^{-1}$, then a substantial asymmetry between red- and blueshifted gas along our line of sight to NGC 7027 must exist. The expansion velocity of the blueshifted high-velocity gas must be only about 19 km s^{-1} , significantly less than the 23 km s^{-1} of the redshifted high-velocity gas. Furthermore, the velocity dispersion of the blueshifted high-velocity gas must be less than that of the redshifted gas to account for the sharp cutoff of emission.

These two requirements are both unlikely. They would imply a more surprising deviation from spherical symmetry than is implied by the geometry sketched in Figure 3, because that geometry retains inversion symmetry about the central star. Differing expansion velocities for the blue- and redshifted high-velocity gas would suggest different mass-loss rates on opposite sides of the central star; such mass loss implies acceleration of the central star away from the center of mass of the nebula.

It is, unfortunately, not easy to estimate the width of the supposed foreground absorption feature, as emission from NGC 7027 is not sufficiently strong at velocities blueshifted from the suspected absorption feature. Careful inspection of our spectra has shown that velocity channels at $v_{\text{lsr}} \leq +2 \text{ km s}^{-1}$ have consistently slightly higher emission than channels at $v_{\text{lsr}} = +4 \text{ km s}^{-1}$; however, this difference is of the order of magnitude of the noise in the spectra.

4.3.6. The v_{lsr} and Expansion Velocity of NGC 7027

Our estimate for the expansion velocity of the neutral envelope is smaller, and our estimate for the v_{lsr} bluer, than that of previous estimates based on the CO $J = 1-0$ line profile (Masson et al. 1985; Knapp & Morris 1985). Since the velocity dispersion is sizable in NGC 7027, and $J = 1-0$ line is moderately optically thick at velocities near the expansion velocity, this line appears broader than twice the expansion velocity. In addition, the presence of some self-absorption at the blueshifted side of the lines redshifts the velocity centroid of the lines from the actual v_{lsr} of NGC 7027. This effect is most prominent in the $J = 3-2$ line, where the self-absorption feature makes the line appear more than 1 km s^{-1} narrower than the $J = 1-0$ line.

One anomaly in the model fits of Figure 5 can be found in the $J = 1-0$ spectra toward large projected radii, especially the one toward $r = 28''$. These spectra have some emission in channels shifted from line center by more than 10 km s^{-1} . If the expansion velocity is still 15 km s^{-1} at these radii, emission at this velocity and projected radius would arise from gas at a radial distance equivalent to $38''$, where, to judge by the $1-0$ data toward a projected radius of $35''$, there should be little or no emission.

There are several possible explanations for the presence of this emission. The expansion velocity could be larger at large radii than at small radii. If the expansion velocity were about 20 km s^{-1} at radii equivalent to about $30''$, then the model fits match the observed line profiles at large projected radii. However, at small projected radii, the fits then put too much emission at velocities shifted about 20 km s^{-1} from line center. This explanation, therefore, requires that CO along our line of sight to the central star be dissociated at radii smaller than $30''$, consistent with the photodissociation radii proposed in § 4.2.4. This possibility is an intriguing one, because larger expansion velocities suggest smaller mass-loss rates; if true, this explanation for the wide $J = 1-0$ line profiles would suggest that the mass-loss rate in NGC 7027 increased 7000–8000 yr ago.

An alternative explanation for the presence of emission at these velocities and projected radii is more prosaic. The $J = 1-0$ data of BWT was created by combining single-dish and interferometer data, in an attempt to recover the flux missing from the interferometer map while retaining its high resolution. This process is a useful one but risks the introduction of some spurious extended flux if the calibrations of the single-dish and interferometer data are inconsistent. It would be valuable to check the $J = 1-0$ line width toward large projected radii by single-dish observations with high resolution ($20''$ would be adequate) in a low-excitation line like CO $J = 1-0$ or perhaps $J = 2-1$.

4.4. Where Is the Carbon?

A puzzle is raised by comparison of the CO:H₂ abundance ratio in the neutral envelope with the C:H and O:H abundance ratios in the ionized region. In the ionized region the C:H ratio has been estimated to be 1.3×10^{-3} , and the O:H ratio to be 4.2×10^{-4} (Perinotto, Panagia, & Benvenuti 1980). A more recent estimate gives a C:H ratio of 2.4×10^{-3} , and an O:H ratio of 6.9×10^{-4} (Zuckerman & Aller 1986). Whatever the exact ratios, the ionized region clearly has a great deal of both C and O, and considerably more C than O. If the elemental abundances are the same in the neutral region as in the ionized region, then our estimate of the CO:H₂ ratio in the neutral region together with Zuckerman & Aller's estimate of the C:H ratio in the ionized region implies that only about 5% of the carbon in the neutral envelope is in CO. This is an implausibly small fraction. No carbon-bearing molecule has been observed that is nearly as abundant as CO. Dust may contain a substantial fraction of the carbon, but the amount of carbon in dust is unlikely to be sufficiently different in the ionized and neutral regions to explain the disparity in observed carbon abundances. There is a significant amount of C II in NGC 7027 (Crawford et al. 1985), but the observed level of emission suggests a mass of C II less than half the mass of CO. C I has been searched for but not yet detected (Beichman et al. 1983) but would have been detected had C I contained a large fraction of the carbon. This is consistent with the typical dis-

tribution of carbon in molecular clouds, where the abundance of C I is always less than that of either C II or CO.

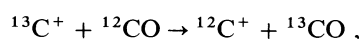
The most plausible explanation for the relatively low CO:H₂ ratio in the neutral region, compared to the high C and O abundances in the ionized region, is a considerable increase in the heavy element abundances, particularly that of carbon, during the last one thousand years of mass loss from the central star. There is some evidence for dramatic changes over short time scales in the elemental abundances in other planetary nebula, for instance in the cases of carbon-rich stars which have oxygen-rich envelopes (Zuckerman & Aller 1986). Such an abundance variation would also help explain the anomalously high heavy element abundances in the ionized region of NGC 7027, compared to other, older planetary nebula which have ionized larger fractions of their envelopes.

NGC 7027 holds promise as a source in which, in time, the evolution of elemental abundances in stellar material lost during the late asymptotic giant branch stage may be observable directly in the envelope. In this way it may be possible observationally to test theories regarding convective mixing in the envelopes of AGB stars. Presently, however, it is not possible to make quantitative estimates of the changes in elemental abundances with radius, partly because of the lack of high spatial resolution observations, and partly because there is so much uncertainty about the fraction of oxygen in dust, H₂O, and O₂, and the fraction of carbon in dust, C I and C II.

4.5. The ¹²C:¹³CO Abundance Ratio

Due to the poor signal-to-noise ratio and more uncertain calibration of our ¹³CO line profiles, we have used the ¹³CO observations chiefly to determine the ¹²CO:¹³CO abundance ratio. The ¹³CO lines cannot be used to estimate physical conditions in the envelope until more reliable line ratios become available. The ¹²CO:¹³CO abundance ratio has long been poorly determined in NGC 7027, largely because of uncertainties regarding the opacities of the ¹²CO lines and the strength of the ¹³CO *J* = 1–0 line. Published estimates of the integrated flux ratio in the *J* = 1–0 lines vary significantly, from 36 ± 6 (Thronson & Mozurkewich 1983) and 40 (Knapp & Chang 1985) to >100 (Sopka et al. 1989). It is now clear from our observations of the higher *J* ¹³CO lines that a ratio of about 40 in the *J* = 1–0 line must be approximately correct. The overall ¹²CO:¹³CO abundance ratio we estimate to be 90 ± 25. This estimate was generated by adapting our model from ¹²CO to ¹³CO, and using the results of the ¹²CO analysis to fix all the model parameters except the ¹²CO:¹³CO abundance ratio.

This ratio is an upper limit to the ¹²C:¹³C abundance ratio, because the ¹³CO is not likely coextensive with the ¹²CO. Because self-shielding from dissociating radiation is so important, ¹³CO is likely to be dissociated to a larger inner radius, and to a smaller outer radius, than is the ¹²CO. According to the calculations of Mamon et al. (1988), at large radii the inferior self-shielding of ¹³CO is nearly balanced by chemical fractionation due to the reaction



which is exothermic by 35 K, and therefore in cold gas dominates the reverse reaction. At the interface with the ionized region in NGC 7027, however, the temperature is greater than 35 K and the effect of this reaction is much less significant. For this reason, ¹³CO may be dissociated to a greater extent than ¹²CO at small radii.

A ¹²C:¹³C abundance ratio as large as 90 is not unreasonable for NGC 7027, although the ratio is significantly smaller in the general interstellar medium. In carbon-rich circumstellar envelopes the ¹²C:¹³C ratio often approaches this magnitude (Lambert et al. 1986). NGC 7027 has a carbon-rich envelope, as the elemental abundances in the ionized region demonstrate.

Deep integration on the ¹³CO lines in NGC 7027 would be valuable in two ways. First, the symmetry of the line profiles would help distinguish between envelope asymmetries and radiative transfer effects as causes of the asymmetry in the ¹²CO *J* = 3–2 line profile. Second, the shape of the line profiles would help determine the extent of the difference in mass-loss rate between the low-density axis and the high-density plane. In a spherically symmetric envelope, the optically thin ¹³CO lines would appear strongly double-peaked in a beam that partially resolves the envelope. If the asymmetry in the mass loss is extreme, the profiles would have a more rounded shape. Our *J* = 2–1 and *J* = 3–2 line profiles have a flattish to rounded profile, which suggests that significantly less ¹³CO lies along our line of sight than along directions orthogonal to our line of sight. This ratio is consistent with our previous estimate that the mass loss rate in the axial direction of NGC 7027 is at least a factor of 2 less than that in equatorial directions.

5. SUMMARY AND PROSPECTS FOR FUTURE WORK

The NGC 7027 neutral envelope was formed by rapid and asymmetric mass loss, with mass-loss rates in equatorial directions corresponding to spherically symmetric mass loss of about 2 × 10⁻⁴ M_⊙ yr⁻¹, and mass-loss rates in polar directions about half that. There is some indication that the mass-loss rate increased as the nebula evolved, but higher resolution observations in several lines and sophisticated modeling will be necessary to demonstrate this. The CO:H₂ ratio is about 2 × 10⁻⁴ and may vary with radius; in most of the envelope this ratio is definitely smaller than would be expected from the C:H and O:H ratios in the ionized region. The extent of the CO emission may be determined by dissociation of the CO by interstellar radiation at radii comparable to or smaller than those predicted by Mamon et al. (1988). Molecular gas at small radii has been strongly perturbed by the ionized region and has obtained large expansion velocities and large velocity dispersion. The quantity of gas which has acquired a large velocity dispersion is larger than that which has been accelerated in expansion velocity. The CO lines have optical depths on the order of or larger than unity, and radiative transfer effects significantly affect the line profiles.

Additional observations can improve our understanding of the NGC 7027 envelope. A better determination of the density at small radii, where currently we are sensitive only to the kinetic temperature and CO abundance, could be made by observations of the CO *J* = 7–6 line, which is likely to be subthermally populated in almost all of the envelope, or by high spatial resolution mapping of the CO *J* = 4–3 line, which may be thermalized to significantly smaller radii than the *J* = 3–2 line. These observations would improve our estimate of the CO:H₂ ratio, which currently is derived from a CO abundance determined at small radii and a mass-loss rate determined at larger radii. High spatial resolution maps in lower excitation lines, such as the CO *J* = 2–1 line, could help uncover the radial dependence, if any, of such parameters as the mass-loss rate, the kinetic temperature, and the CO:H₂ ratio. Improved observations of the ¹³CO lines would help

determine both the importance of radiative transfer effects and the degree of asymmetry in the mass loss. High-resolution observations of the C I lines would help resolve questions regarding the carbon abundance. The nature of the largely atomic interface region between the ionized and molecular gas is poorly understood; it is probably dense and hot, and high spatial resolution observations of highly excited molecular lines could be very helpful in probing this region. The velocity structure of the gas near the ionized region is complex, and high spatial resolution observations will be necessary to understand it.

Our model calculation of NGC 7027 can also be improved. The foremost weaknesses of our model are, first, its assumption of spherical symmetry, and, second, its assumption of large velocity gradients. Given the large velocity dispersion in NGC 7027, radiative transfer of CO line photons from smaller radii may affect the level populations at large radii. An explicitly aspherical model would help to understand the extent and

nature of the envelope asymmetry. Improved model calculations will become more important as the available observational data grows.

The authors are grateful to Harley Thronson for sharing the $J = 1-0$ data used in this paper. We would like to thank the staff of the James Clerk Maxwell Telescope for their hospitality. The James Clerk Maxwell Telescope is operated by the Royal Observatory, Edinburgh on behalf of the Science and Engineering Research Council of the United Kingdom, the Netherlands Organization for Scientific Research, and the National Research Council of Canada. This work has been supported by the National Science Foundation under grants AST-8818327 and AST-9196077. P. A. Jaminet was supported by a NASA Graduate Student Research Program Fellowship during the period of this work, and W. C. Danchi received partial support from the L. W. Frohlich Research Fellowship of the New York Academy of Sciences.

APPENDIX

DETAILS OF THE MODEL CALCULATION

1. STATISTICAL EQUILIBRIUM BETWEEN LEVELS

At each radius r from the central star we calculate the populations of the CO rotational levels. For this purpose, radiative transfer is treated using the Sobolev (large velocity gradient) approximation in which absorption and stimulated emission can occur only in a localized region over which physical parameters, such as density and kinetic temperature, are uniform. The circumstellar envelope is assumed spherically symmetric. The equations of statistical equilibrium were essentially those used by Goldreich & Kwan (1974) and de Jong, Chu, & Dalgarno (1975) for a uniformly expanding envelope, with a few differences which we describe below.

For the external sources of radiation at CO line frequencies, we included contributions from the cosmic microwave background, cold dust in the extended neutral envelope with $\tau_{\text{cd}} \approx 0.002(\nu/800 \text{ GHz})$ and $T_{\text{cd}} \approx 20 \text{ K}$ (Gee et al. 1984), and free-free emission from the ionized region for which we assumed a flux density as seen from Earth equal to 4.3 Jy, independent of frequency (Gee et al. 1984). Other sources of millimeter and submillimeter wavelength continuum are small. We entirely neglected the effects of absorption and scattering by dust. These effects are small, because the dust opacities at the CO line frequencies are small compared to both unity and the CO line opacities. We have also neglected the effects on the level populations due to pumping at the $4.6 \mu\text{m}$ CO $v = 1-0$ fundamental vibrational transition. The continuum flux from NGC 7027 in the mid-infrared (e.g., Arens et al. 1984) is less than that required to significantly affect the CO level populations (Carroll & Goldsmith 1981).

The collisional rate coefficients for deexcitation of CO by H_2 were taken from the literature, after which the upward collisional rate coefficients were obtained through detailed balance:

$$\gamma_{J',J}(2J' + 1) = \gamma_{J,J'}(2J + 1)e^{-\Delta E/kT_{\text{kin}}}, \quad J > J'.$$

The best available rates for CO deexcitation due to collisions with para- H_2 are probably those of Schinke et al. (1985), but we have instead used the rates of Flower & Launay (1985), who calculated rates for collisions with both para- and ortho- H_2 . We assumed 75% ortho- H_2 and 25% para- H_2 .

Since kinetic temperature affects the collision rates and thereby the calculated brightness temperatures of the CO lines, it is necessary to assign a kinetic temperature at each radius. We used a power law for the kinetic temperature, with the exponent and the value of the kinetic temperature at a reference radius free parameters. We interpolated between published deexcitation rates to find the collision rates at the appropriate kinetic temperature. For kinetic temperatures below 10 K, we used the 10 K deexcitation rates. The deexcitation rates are not strongly dependent on kinetic temperature, as the excitation rates are, and this approximation probably has little effect on the calculation.

2. BRIGHTNESS TEMPERATURES AND LINE PROFILES

Once the density of CO in each rotational level and at each radius is known, model line profiles can be calculated exactly. The calculation has two steps: first, the computation of a brightness temperature distribution on the sky, and second, the convolution of this distribution with a model telescope beam. The equations presented here are adapted from those of Morris, Lucas, & Omont (1985).

The brightness temperature toward a point on the sky at a projected radius p from the nebular center is

$$T_J(p, v) = \int_{-\infty}^{\infty} dz' K_J(p, z', v) T_s(p, z') \exp \left[- \int_{z'}^{\infty} K_J(p, z'', v) dz'' \right] + (e^{-\tau_1(p, v)} - 1) \frac{h\nu_J/k}{e^{h\nu_J/kT_{bg}} - 1} \\ + (e^{-\tau_2(p, v)} - 1) \frac{c^2}{2k\nu_J^2} F_\nu D^2 \frac{\Delta z}{(4\pi/3)(r_{out}^3 - r_{in}^3)}.$$

Here the absorption coefficient $K_J(p, z, v)$ and the source function $T_s(p, z)$ are as given by Morris et al. (1985).

The last two terms in the equation for $T_J(p, v)$ arise due to the subtraction of continuum emission from the observed spectrum during data acquisition and analysis. This subtraction does not eliminate the influence of continuum emission on the line profiles, because nebular CO obscures the continuum emission at the CO line velocities. The first term accounts for the cosmic microwave background; $\tau_1(p, v)$ is the total optical depth the model nebula presents to the cosmic microwave background. The last term accounts for continuum radiation from the ionized region; $\tau_2(p, v)$ is the optical depth of the nebular CO between us and the ionized region, $F_\nu = 4.3$ Jy is the flux of the ionized region seen from Earth, and D is the distance of NGC 7027. We have approximated the continuum emission as optically thin emission from a homogeneous spherical shell with outer radius $r_{out} = 3''.8$ and inner radius $r_{in} = 2''.5$ (Masson 1989). Self-absorption in the ionized region and absorption by the ionized gas against the redshifted CO emission are ignored. In this approximation the ionized region emission along a given line of sight is proportional to

$$\Delta z = \begin{cases} 0 & p > r_{out} \\ 2\sqrt{r_{out}^2 - p^2} & r_{in} < p < r_{out} \\ 2\sqrt{r_{out}^2 - p^2} - 2\sqrt{r_{in}^2 - p^2} & p < r_{in} \end{cases}.$$

The continuum contribution to the observed line profile is most significant in the $J = 1-0$ line, because the Rayleigh-Jeans brightness temperatures of both the cosmic microwave background and the NGC 7027 continuum fall with increasing frequency.

The main-beam brightness temperature at the velocity v observed by a telescope with symmetric beam response function G pointed toward a projected radius p_0 from the central star is

$$T_J(v) = \int_0^{2\pi} d\phi \int_0^\infty p dp G(p') T_J(p, v),$$

where p' , the separation between the emitting point and the point at the center of the telescope beam, is given by

$$p'^2 = p^2 + p_0^2 - 2pp_0 \cos \phi.$$

For a telescope with a Gaussian beam of full width half-maximum B ,

$$G(p) = \frac{4 \ln 2}{\pi B^2} \exp \left(\frac{-p^2 4 \ln 2}{B^2} \right).$$

The integrals are calculated numerically. The integrals were cut off at a maximum radius r_{max} at which the CO was assumed to be largely dissociated. The central cavity, where no CO exists, was taken to be spherical with a radius $r_{min} = 4''.5-5''.5$. We assume a discontinuous transition between atomic and molecular gas; as the transition region is known to be small compared to our spatial resolution, this approximation is unlikely to degrade our results.

REFERENCES

- Arens, J. F., Lamb, G. M., Peck, M. C., Moseley, H., Hoffmann, W. F., Tresh-Fienberg, R., & Fazio, G. G. 1984, *ApJ*, 279, 685
 Atherton, P. D., Hicks, T. R., Reay, N. K., Robinson, G. J., Worswick, S. P., & Phillips, J. P. 1979, *ApJ*, 232, 786
 Basart, J. P., & Daub, C. T. 1987, *ApJ*, 317, 412
 Beichman, C. A., Keene, J., Phillips, T. G., Huggins, P. J., Wootten, H. A., Masson, C. R., & Frerking, M. A. 1983, *ApJ*, 273, 633
 Bieging, J. H., Wilner, D., & Thronson, H. A. 1991, in preparation (BWT)
 Carroll, T. J., & Goldsmith, P. F. 1981, *ApJ*, 245, 891
 Crawford, M. K., Genzel, R., Townes, C. H., & Watson, D. M. 1985, *ApJ*, 291, 755
 Cox, P., Gusten, R., & Henkel, C. 1987, *A&A*, 181, L19
 Deguchi, S., Izumiura, H., Kaifu, N., Mao, X., Nguyen-Q-Rieu, & Ukita, N. 1990, *ApJ*, 351, 522
 de Jong, T., Chu, S.-I., & Dalgarno, A. 1975, *ApJ*, 199, 69
 Flower, D. R., & Launay, J. M. 1985, *MNRAS*, 214, 271
 Gammie, C. F., Knapp, G. R., Young, K., Phillips, T. G., & Falgarone, E. 1989, *ApJ*, 345, L87
 Gee, G., Emerson, J. P., Ade, P. A. R., Robson, E. I., & Nolt, I. G. 1984, *MNRAS*, 208, 517
 Goldreich, P., & Kwan, J. 1974, *ApJ*, 189, 441
 Kawabe, R., et al. 1987, *ApJ*, 314, 322
 Knapp, G. R., & Chang, K. M. 1985, *ApJ*, 293, 281
 Knapp, G. R., & Morris, M. 1985, *ApJ*, 292, 640
 Kwan, J., & Linke, R. A. 1982, *ApJ*, 254, 587
 Lambert, D. L., Gustafsson, B., Eriksson, K., & Hinkle, K. H. 1986, *ApJS*, 62, 373
 Mamon, G. A., Glassgold, A. E., & Huggins, P. J. 1988, *ApJ*, 328, 797
 Masson, C. R. 1989, *ApJ*, 336, 294
 Masson, C. R., et al. 1985, *ApJ*, 292, 464
 Morris, M., Lucas, R., & Omont, A. 1985, *A&A*, 142, 107
 Mufson, S. L., Lyon, J., & Marionni, P. A. 1975, *ApJ*, 201, L85
 Oloffson, H., Johansson, L., Nguyen-Q-Rieu, Sopka, R. J., & Zuckerman, B. 1982, *BAAS*, 14, 895
 Perinotto, M., Panagia, N., & Benvenuti, P. 1980, *A&A*, 85, 332
 Phillips, J. P., White, G. J., & Richardson, K. J. 1985, *A&A*, 151, 421
 Pottasch, S. R., Goss, W. M., Arnal, E. M., & Gathier, R. 1982, *A&A*, 106, 229
 Schinke, R., Engel, V., Buck, U., Meyer, H., & Diercksen, G. H. F. 1985, *ApJ*, 299, 939
 Schonberg, K. 1988, *A&A*, 195, 198
 Sopka, R. J., Oloffson, H., Johansson, L. E. B., Nguyen-Q-Rieu, & Zuckerman, B. 1989, *A&A*, 210, 78
 Spitzer, L., Jr. 1978, *Physical Processes in the Interstellar Medium* (New York: John Wiley & Sons), 220
 Sutton, E. C., Danchi, W. C., Jaminet, P. A., & Ono, R. H. 1990, *Internat. J. Infrared Millimeter Waves*, 11, 133
 Thronson, H. A., & Bally, J. 1986, *ApJ*, 300, 749
 Thronson, H. A., & Mozurkewich, D. 1983, *ApJ*, 271, 611
 Tielens, A. G. G. M., & Hollenbach, D. 1985, *ApJ*, 291, 722
 Treffers, R. R., Fink, U., Larson, H. P., & Gautier, T. N., III. 1976, *ApJ*, 209, 793
 Vallee, J. P., Guilloteau, S., Forveille, T., & Omont, A. 1990, *A&A*, 230, 457
 Zuckerman, B., & Aller, L. H. 1986, *ApJ*, 301, 772